Solar Energy Materials & Solar Cells 269 (2024) 112789

Contents lists available at ScienceDirect

Solar Energy Materials and Solar Cells

journal homepage: www.elsevier.com/locate/solmat

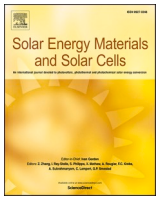

Light-activated surface passivation for more efficient silicon heterojunction solar cells: Origin, physics and stability

Fiacre E. Rougieux [a,*,1], Chandany Sen [a,1], Malcolm Abbott [b], Bram Hoex [a]

[a] School of Photovoltaic and Renewable Energy Engineering, University of New South Wales, Sydney, NSW, 2052, Australia
[b] PV Lighthouse, Australia

ARTICLE INFO

Keywords:
Recombination
Surface passivation
Degradation
HJT solar cells
Interface defect density
Charge
Defects
Silicon
Field effect
Reliability
Modelling surface recombination

ABSTRACT

Silicon heterojunction (HJT) solar cells have world-leading efficiencies due to outstanding surface passivation. Yet, maintaining their performance during the lifetime of a photovoltaic module requires excellent quality and stability of the surface regions. It is well known that HJT solar cells can show an increase or reduction in performance under illumination, and this instability has been related to changes in the surface regions. This work investigates the stability of surface passivation in HJT solar cells by modelling the injection-dependent minority carrier lifetime of a range of symmetrically a-Si passivated silicon wafers. Fixed charges and defects at the interface are varied in the model to find the best fit to the injection-dependent lifetime before and after a high-intensity illumination treatment. The results indicate that the laser process induces an increase in field effect passivation at the surface, which is then reduced upon storage in the dark. The results show that lifetime spectroscopy is a useful tool to investigate the nature of a-Si passivation degradation.

1. Introduction

A key advantage of the heterojunction (HJT) architecture is its ability to yield open circuit voltages (V_{OC}) exceeding 750 mV and fill factors (FF) approaching 90% [1]. However, achieving this in mass production while ensuring long-term stability when deployed in the field is a formidable challenge. The device architecture relies on extremely high-quality electrical passivation of the surfaces, and any changes to that complex structure can result in a subsequent reduction in efficiency (i.e., long-term instability). The key to overcoming this challenge is understanding the interface properties better and how they may change in response to processing and exposure to field conditions. The nature of the mechanisms limiting the passivation quality of a-Si passivation was intensely studied in the early 2010s. However, with an order-of-magnitude improvement in surface passivation since the 2010s, this calls for a reexamination of the issue.

More recently, silicon heterojunction performance has been shown to increase after an illuminated anneal, manifested as an increase in V_{OC} [2]. Efficiency gains of 0.3% absolute [2] and 0.4% absolute [3] were reported, with the increase attributed to an improved passivation of the c-Si/a-Si interface. In current industrial HJT solar cells, it is unclear whether this improvement is related to the i/n-Si or i/p-Si layer and if so, it is unclear if it is caused by interface defects [4–7] or field effect passivation [8,9]. In addition, subsequent work has shown that this improvement is not stable, with Yang et al. showing a decrease in the open circuit voltage after dark annealing at elevated temperatures [10]. That work did not provide any detailed physical explanations of the mechanisms, particularly relating to possible changes in the fixed charge, field effect or interface defects at the surface. This calls for re-evaluating the physics of surface passivation degradation in HJT cells, particularly where those cells have received a performance boost due to post-processing, high-intensity irradiation treatments. Critical to this is the development and validation of techniques to enable better sample characterization, particularly of these surface regions. Traditional methods of measuring interface defects or surface charge in dielectric passivating films, such as capacitance-voltage measurements cannot be used to measure a conductive a-Si contact. The degradation is, however, noticeably clear when measuring the injection-dependent effective minority carrier lifetime (referred to as lifetime from now onwards). By fitting lifetime measurements with a detailed model, one could, in principle, infer the relative impact of defect densities and field-effect on the passivation quality.

* Corresponding author.
E-mail address: fiacre.rougieux@unsw.edu.au (F.E. Rougieux).
[1] Equal first authorship.

https://doi.org/10.1016/j.solmat.2024.112789
Received 28 November 2023; Received in revised form 23 February 2024; Accepted 23 February 2024

Historically, the challenge for modelling has been to describe both the recombination rate and associated charge properties at the interface precisely. Initially, Garin et al. [11] used a model of the surface recombination rate, making use of fixed a-Si charges and charged interface defects with occupancy described by the Shockley-Read-Hall theory [12,13]. However, dangling bond states, which drive surface recombination, have three different charge conditions. The Shockley-Read-Hall theory is thus not applicable for such defects, as it only describes monovalent defects (defects with two charge states). Olibet et al. [14] suggested modifications to that effect, but their description was limited to using an approximate expression of the recombination rate [15]. The recombination rate of multivalent defects is well described by the formulation of Sah and Shockley [16], and this recombination rate was successfully used by Leendertz et al. [17,18] to describe recombination at dangling bonds in a-Si. Leendertz et al. demonstrated [18] that modelling the recombination rate via a Gaussian distribution of states with three charge states (two energy levels correlated by an energy of 0.15 eV) is superior to previous approaches by comparing to AFORS-HET simulations [17] and experimental measurements. This paper essentially uses this modelling approach together with a fit optimisation method to obtain charge density and interface defect density parameters from lifetime measurements. The results of this process are used to explain the changes in surface passivation during illuminated annealing of heterojunction solar cells.

In this paper, we provide a possible explanation of the origin and the physics of increases in open circuit voltage and implied fill factor of heterojunction solar cells following illuminated annealing. Using advanced lifetime spectroscopy analysis, we show that this approach is only partially stable and that its lack of stability stems from a progressive reduction in the field effect passivation.

2. Sample preparation

The samples used in this study were n-type Czochralski (Cz) grown wafers with a thickness of 140 μm and a resistivity of 2 Ω cm sourced from an industrial production line. To study the nature of passivation degradation, the samples were divided into five groups as shown in Table 1.

Group 1 - HJT cell: These cells had an n-type wafer with intrinsic hydrogenated amorphous silicon (i-a-Si:H) passivation layers on both sides. The front and rear sides had phosphorus-doped (n-a-Si:H) and boron-doped (p-a-Si:H) hydrogenated amorphous silicon layers, respectively. Additionally, an indium-doped tin oxide (ITO) layer ~ 80 nm thick was deposited on both sides, and a screen-printed H-pattern silver grid was printed on both sides of the cells. Group 2 - Cell precursor: The samples in this group featured an n-type wafer with i-a-Si:H passivation layers on both sides. The front and rear sides had n-a-Si:H and p-a-Si:H passivation layers, respectively. Group 3 - i/n-Si symmetrical lifetime test structure: This group featured an n-type wafer with i-a-Si:H and n-a-Si:H layers on both sides. Group 4 - i/p-Si symmetrical lifetime test structure: This group featured an n-type wafer with i-a-Si:H and p-a-Si:H layers on both sides. Group 5 - i-Si symmetrical lifetime test structure: This group featured an n-type wafer with i-a-Si:H. The thickness of i-a-Si:H, n-a:Si:H and p-a:Si:H layers of samples in all groups were about 5 nm. This preparation allows the separation of the role of different layers (intrinsic, doped) on passivation instabilities. All deposition processes were carried out at the industrial production line. The samples received an illuminated anneal at 175 °C with a laser intensity of approximately 6 W cm^{-2} for 30 s on the front side (the side with n-a-Si:H passivation layer) and then stored in the dark at room temperature for several weeks. It is important to note that no substantial changes were noticed when illuminated annealing was done from the rear side (the side with p-a:S:H) in all groups. Therefore, these results were excluded from this study. The lifetime was measured using transient photoconductance with a Sinton WCT120 system. The lifetime was modelled based on previously published work [17,18], with a surface recombination velocity model assuming a Gaussian distribution of defect states centred around midgap where the defects are multivalent (three charge states) dangling bonds. The fit of the lifetime provides insight into the possible evolution of the interface defect density and the field-effect passivation component during degradation.

Table 1
Structures of the five sample groups used in this study.

Sample	i-layer	n-layer	p-layer	metals
Group 1	yes	yes	yes	yes
Group 2	yes	yes	yes	no
Group 3	yes	Yes both sidess	no	no
Group 4	Yes	no	Yes both sides	no
Group 5	yes	no	no	no

3. Lifetime fitting methodology

3.1. Modelling recombination

Defects at the a-Si/Si interface can capture electrons and holes, thus acting as recombination centres, limiting the lifetime. Reducing the interface defect density improves the chemical passivation component of surface passivation. Doping of the a-Si induces band bending at the a-Si/Si, leading to field effect passivation. In the context of a-Si surface passivation, the charge is a metric that captures the field-effect passivation.

This paper aims to separate the changes in surface recombination due to (1) changes in field-effect passivation (i.e. changes in surface charge) and (2) changes in degradation due to chemical passivation (i.e. changes in the number of interface defects). To this effect, we calculate the surface recombination rate as a function of the charge and the interface defect density distribution by applying the method described in [19–21]. This fitting procedure is the most advanced lumped-parameter modelling procedure and has been successfully applied to model amorphous silicon passivation. To calculate the recombination rate requires the electron and hole concentration near the a-Si/Si interface n_s and p_s [22]:

$$n_s = n_d \, exp\left(\frac{-\psi_S}{kT}\right), p_s = p_d \, exp\left(\frac{\psi_S}{kT}\right) \tag{1}$$

where n_d and p_d are the electron and hole carrier concentrations deep in the wafer bulk (where the energy band is flat) and ψ_S is the surface potential.

Numerically solving the charge neutrality equation allows the calculation of the surface concentrations [22]:

$$p_S + n_S - p_d - n_d + (N_A + N_D)\frac{\psi_S}{kT} = \frac{Q^2}{2q\varepsilon_{Si}kT} \tag{2}$$

where ε_{Si} is the dielectric constant of Si, q is the fundamental electric charge and Q is the total charge concentration. The charge concentration is the sum of the charges in the a-Si, at the interface and in the space-charge region of the crystalline silicon wafer. There are two approaches to treat charges; 1) calculating the full injection-dependent charge distribution in the a-Si and at the interface or 2) assuming an injection-independent fixed charge concentration. Both yield comparable results especially at injection above 10^{14} cm^{-3} [18], and to speed up numerical simulations, we follow the second approach and simulate charges as injection-independent fixed charges.

Fig. 1 illustrates the physics of recombination at dangling bonds at the silicon/amorphous silicon interface [17,18]. Dangling bonds have three charge states (thus four different capture coefficients), where the two energy levels are separated by a correlation energy U [23]. For modelling the surface recombination rate, we use an energy-dependent defect density (a Gaussian distribution centred at midgap) [23,24] and

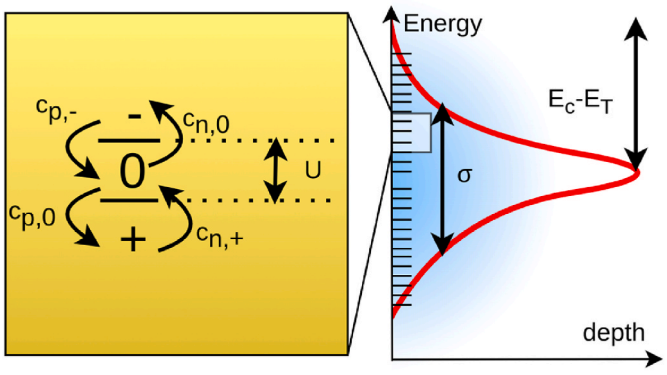

Fig. 1. Illustration of the models for silicon dangling bonds at the silicon/amorphous silicon interface.

energy-independent capture rates ($c_{n,+}$, $c_{n,0}$, $c_{p,0}$, $c_{p,-}$) which allow calculation of an energy-dependent recombination rate [25]. Integration of this recombination rate over the bandgap enables the calculation of the recombination velocity S [26], which is subsequently used to calculate the effective lifetime:

$$\tau_{eff} = \frac{1}{1/\tau_{int} + 1/\tau_{bulk} + 1/\tau_{surf}} \text{ with } \tau_{surf} = \frac{W}{2S} \quad (3)$$

With τ_{int} the intrinsic lifetime (i.e., Auger and band-band radiative), τ_{bulk} is the wafer bulk SRH lifetime (here assuming an injection independent lifetime of $\tau_{bulk} = 25$ ms, where the bulk has virtually no impact on the measured lifetime here). The model was validated against previous models from [17,18] and we use all the parameters of [18].

3.2. Illustration of the method

Key to the method is the fact that the charge and interface defect density have different impacts on the injection dependent lifetime. The series of theoretical curves shown in Fig. 2 demonstrates how changes in (a) the total charge at the surface and (b) the maximum interface defect density (D_{it}) result in differences in the injection-dependent effective lifetime.

An increase in charge results in an increase in the injection dependent minority carrier lifetime, especially at low injection. On the other hand, an increase in D_{it} leads to a uniform reduction in the injection-dependent lifetime. From the shape of the injection-dependent lifetime curve, fundamental information about D_{it} and charge can be inferred. Note that determining the absolute values of D_{it} and fixed charge from lifetime spectroscopy is challenging as their values will depend on the assumption of the defect parameters: capture parameters $c_{n,+}$, $c_{n,0}$, $c_{p,0}$, $c_{p,-}$, correlation energy U, gaussian distribution centre E_C-E_T and gaussian distribution width. Figure A1 in the appendix shows that a deeper defect, or one with a wider defect distribution, also leads to a uniform decrease in the lifetime. In addition, Figure A2 in the appendix shows that a larger charge capture cross section leads to an injection-dependent decrease in the lifetime and a larger correlation energy an injection-dependent increase in the lifetime.

While determining absolute values of D_{it} and charges are challenging, tracking their relative changes during processes (illumination, annealing, dark storage …) is possible provided one assumes that the defect parameters remain constant during processes and only the charge and defect density change. The values presented in graphs below thus assume the values from [17,18] apply to our sample.

3.3. Inferring charge and interface properties via fitting optimisation

Determining the charge and interface defect density from the lifetime curve is an inverse problem. In other words, we are trying to determine the cause or inputs (interface defect density and charge concentration) based on observed effects or outputs (injection-dependent minority carrier lifetime). To achieve this, we fit the lifetime curve with the models described in Section 3.1 and calculate the Root Mean Square Error (RMSE). We optimise the parameters (charge and interface defect density) by minimising the RMSE to below a suitable threshold. We use the Nelder-Mead optimisation method to find the minimum for its ability to converge rapidly to low RMSE (believed to be the global minimum) [27]. The only variables during fitting were the max interface defect concentration and the charge. A typical solution space for that type of fitting is shown in Appendix 4.

Note that during all the simulations, we keep all defect parameters constants (capture parameters $c_{n,+}$, $c_{n,0}$, $c_{p,0}$, $c_{p,-}$, correlation energy U, gaussian distribution centre E_C-E_T and gaussian distribution width) with the values from [17,18]. Obviously, changing the defect parameters when the lifetime evolves would allow for a perfect fit for every sample. This approach is, however, nonphysical and against the purpose of our goal here as we intend to extract meaningful information from our fitting.

4. Results and discussion

4.1. Efficiency improvements post laser annealing in heterojunction solar cells

Fig. 3 shows the evolution of the a) current voltage curve of a heterojunction cell and b) injection dependent minority carrier lifetime of a heterojunction cell precursor before and after treatment. The laser

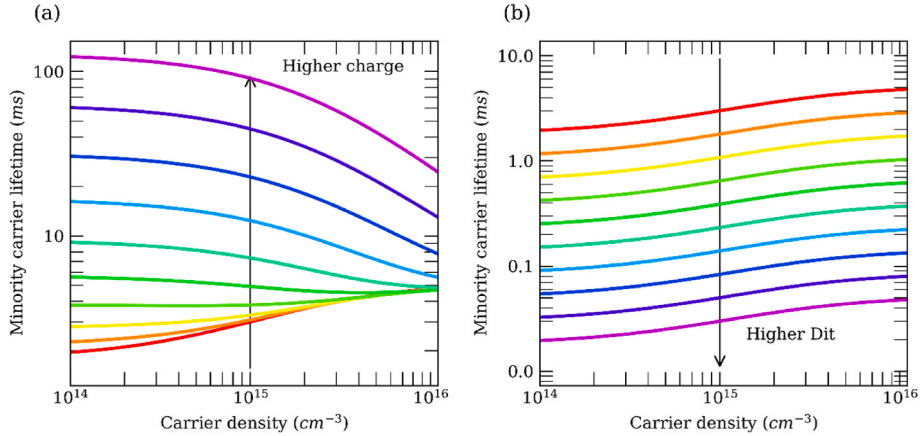

Fig. 2. Impact of a) the charge concentration and b) the interface defect density on the injection dependent minority carrier lifetime.

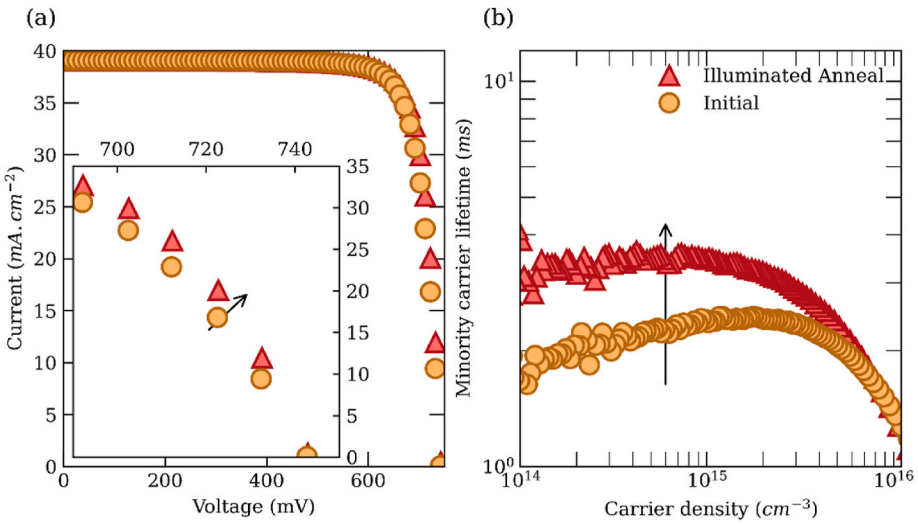

Fig. 3. a) Current-voltage curve of a heterojunction cell and b) injection-dependent minority carrier lifetime of a heterojunction cell precursor before and after treatment.

process leads to a visible improvement of the cell efficiency (23.8%–24.4%) due to an increase in both open circuit voltage (742.8 mV–743.1 mV) and fill factor (82.3%–83.6%). The change in open circuit voltage is due to an increase of the lifetime at medium/high injection. The increase in fill factor is partly driven by a change in the injection-dependent lifetime curve, which becomes flat at low injection instead of going down.

Having shown the improvements achieved using illuminated annealing, we proceed to look at where they originate from using symmetrically passivated structures.

4.2. Efficiency improvements are driven by both an increase in field effect passivation and chemical passivation of the i/n-Si layer

4.2.1. Measured light and elevated temperature surface passivation improvement of the i/n-Si layer

Fig. 4 shows the injection-dependent lifetime of a sample with a) i/n-Si stack and b) i/p-Si stack before and after illuminated annealing. The minority carrier lifetime of the i/n-Si passivated samples increases significantly whilst the lifetime of the i/p-Si remains almost constant. This indicates that efficiency improvements in such cells are driven by changes in the i/n-Si contact not the i/p-Si contact or the bulk.

Note that the fit quality, though reasonable, could be improved with more accurate input parameters. In particular, the interface defect density distribution, capture cross section and correlation energy could be measured directly on the sample instead of taken from the literature). This could be done via transient capacitance spectroscopy techniques (electrically, optically or thermally stimulated) on a-Si transistors (not diodes as i-Si/Si contacts are conductive).

The results of the lifetime measurement indicate that the efficiency enhancements originate from the i/n-Si layer. The results of the lifetime curve fitting, shown in Table 2 below, provide some insight into the physical reason for this. Figure A3 in the appendix, shows the solution space for charge and interface defect density and gives an indication of the uncertainty of these two quantities. For all our samples we find that the relative uncertainty remains small except when either the interface defect density or charge become very small in which case the

Table 2
Fitting results (charge and interface defect density) and RMSE.

Sample	Condition	Q (cm^{-2})	D_{it} (cm^{-2})	RMSE (a.u.)
i-n/Si	**Initial**	-4.15×10^{10}	2.51×10^{10}	1.13×10^{-01}
i-n/Si	**Post Process**	-4.11×10^{11}	9.61×10^{10}	7.75×10^{-02}
i-p/Si	**Initial**	1.01×10^{11}	2.74×10^{11}	2.40×10^{-01}
i-p/Si	**Post Process**	2.25×10^{11}	7.36×10^{11}	4.1×10^{-02}

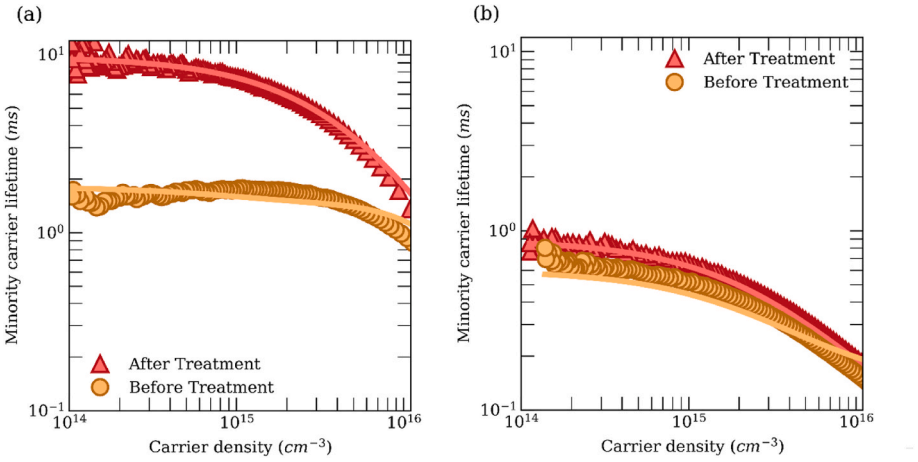

Fig. 4. Injection-dependent minority carrier lifetime before and after illuminated anneal for an a) i/n-Si passivated sample and for a b) i/p-Si passivated sample. The line is the modelled lifetime used to extract changes in charge and interface defect density.

uncertainty becomes large due to the lifetime being insensitive to these parameters.

The fit in Fig. 4 provides a general trend on the evolution of the charge and interface defect density based on the lifetime. The analysis of the injection dependent lifetime spectroscopy data using the method introduced in Section 3.3. reveals that the most likely explanation for the increase in lifetime in the i/n-Si passivated sample is a combination of a fivefold decrease in the intrinsic defect density combined with a tenfold increase in the effective charge.

4.2.2. Possible mechanism for selective chemical passivation improvement

A possible mechanism for the enhancement of chemical passivation is due to the migration of hydrogen to the surface during illuminated annealing [28]. The migration of hydrogen leads to the passivation of dangling bonds which reduces the interface defect density and improves the chemical passivation [29].

The fact that this effect only occurs for the n-type layer could be related to the charge transition levels of hydrogen being in or close to the upper half of the bandgap ($E_D = E_C - 0.16$ eV and $E_A = (E_C + E_V)/2 - 0.064$ eV) and the fundamental difference between the c-Si:i/n-Si interface and the c-Si:i/p interface. The c-Si:i/p-Si interface is in inversion [30], with the Fermi level close to the valence band and at thermal equilibrium, H^+ is thus the majority species [31]. The c-Si:i/n-Si interface is in accumulation [30] with the Fermi level close to the conduction band and at thermal equilibrium in the dark H^- is thus the majority species [31]. During annealing the fermi level moves towards mid-gap due to an increase of the intrinsic carrier concentration. For c-Si:i/p-Si, this means little change as H^+ remains the dominant species, while for c-Si:i/n-Si an increasing fraction of the interstitial hydrogen becomes H^+ [31]. This trend still holds under illumination, though now the fraction of neutral hydrogen increases (but remains well below that of H^+ [31].

If hydrogen passivation is driven by coulombic interaction, it is challenging to happen during illuminated annealing at the c-Si:i/p-Si interface. Indeed, both hydrogen and most dangling bonds are in a positive charge state. Conversely, at the c-Si:i/n-Si interface, under conditions of high temperature and illumination, a considerable proportion of dangling bonds assume a negative charge state and hydrogen adopts a positive charge state, potentially facilitating hydrogen passivation.

4.2.3. Possible mechanism for field effect passivation improvement

Illuminated annealing can improve the conductivity (dark and photo) of amorphous silicon films [32]. This has been attributed to a decrease of acceptor state concentration in amorphous silicon [32], leading to a shift of the Fermi level upwards (decrease in doping in p-type and increase in n-type). This increase in n-type doping would increase the band bending in the silicon and thus the field effect passivation.

In the next section, we will show that these improvements are partly unstable and explore the nature of instabilities in this passivation stack.

4.3. Dark degradation of surface passivation is driven by a loss of field effect passivation

Fig. 5a shows the injection-dependent lifetime of a sample with i/n-Si stack after different lengths of time in dark storage. The fit parameters in Fig. 5b show that the charge decreases significantly during dark storage. The interface density (not shown here) remains almost constant (±12% which is within the uncertainty of the technique) during dark storage.

The lifetime of the i/p-Si passivated sample does not change after dark storage and is thus not shown here (See appendix A0.3). The lifetime of the i-Si passivated sample decreases significantly during dark storage and this is explored in the next section.

4.4. The instability of intrinsic a-Si degradation after treatment is driven by loss of chemical passivation

Fig. 6a shows the injection-dependent lifetime of a sample with i-Si after different lengths of time in dark storage. Unlike the i/n-Si stack, the i-Si passivation stack does not provide any field effect passivation due to the lack of dopants in the amorphous layer. The loss in charge (either interface or a-Si charge) observed for the i/n-Si stack can thus not explain the decrease in surface passivation quality. This is confirmed in Fig. 6b, showing that the decline in surface passivation quality is explained by an increase in interface defect density following dark storage. The decrease in lifetime has been observed before, and because the samples are stored in the dark, dark degradation of surface passivation cannot be explained by the Staebler-Wronski effect [33].

5. Conclusion

This work confirms that implementing an illuminated annealing process can increase the efficiency of heterojunction solar cells. Based on measurements taken from the lifetime test structure, it has been observed that the improvement results from enhanced passivation of the i/n-Si layer. This has led to an increase in fill factor from 82.3% to 83.6% and a slight rise in the open circuit voltage from 742.8 mV to 743.1 mV after an illuminated annealing process. Based on measurements on

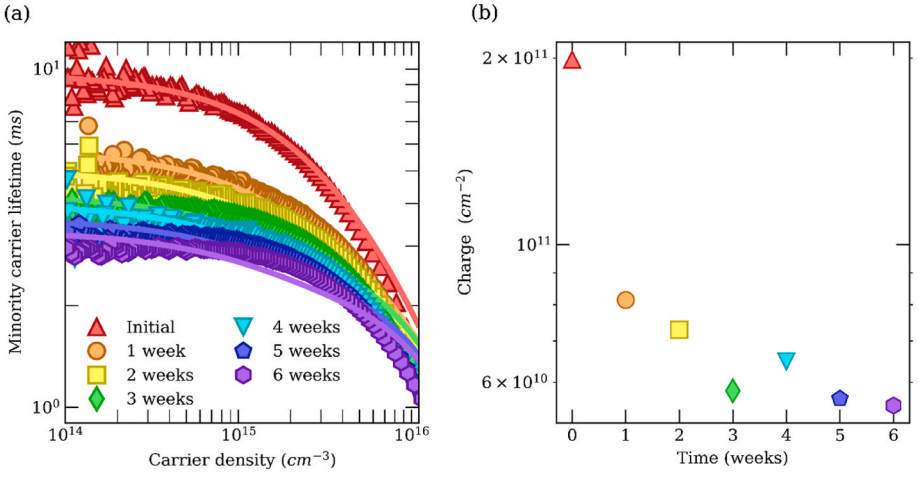

Fig. 5. i/n-Si: Evolution of a) the injection dependent minority carrier lifetime and b) the charge for a sample after laser processing after different length of storage in the dark. The line is the modelled lifetime used to extract changes in charge and interface defect density.

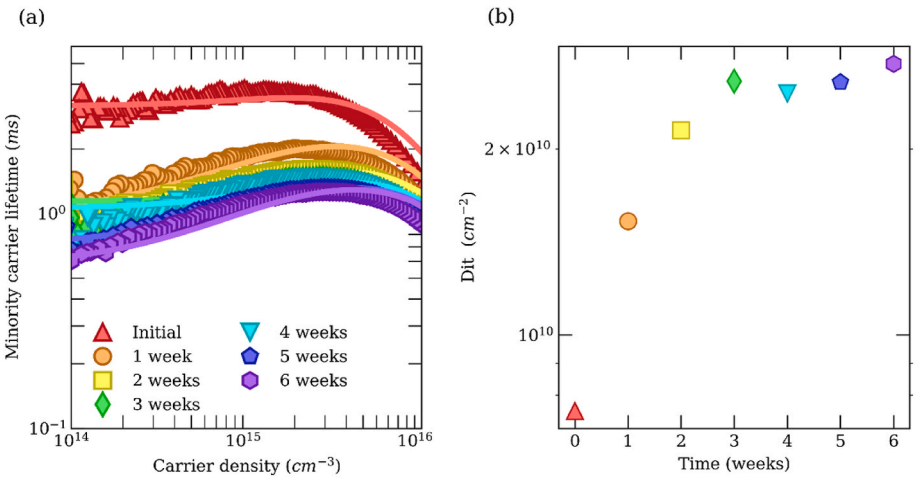

Fig. 6. i-Si: Evolution of a) the lifetime and b) the intrinsic defect density for a sample after laser processing after different length of storage in the dark. The line is the modelled lifetime used to extract changes in charge and interface defect density.

lifetime test structures, the improved passivation leads to a change of the shape of the injection-dependent lifetime, yielding an improved fill factor.

Modelling suggests that this improved passivation will likely stem from a fivefold decrease in the intrinsic defect density combined with a tenfold increase in the effective charge in the i/n-Si layer. We also demonstrate that this improvement is partly temporary due to a subsequent decrease in the charge. Field-effect passivation has a stable component and a temporary component. Our results show that passivation engineering must consider both permanent and temporary passivation mechanisms.

CRediT authorship contribution statement

Fiacre E. Rougieux: Writing – review & editing, Writing – original draft, Visualization, Validation, Software, Resources, Methodology, Investigation, Funding acquisition, Formal analysis, Data curation, Conceptualization. **Chandany Sen:** Writing – review & editing, Resources, Methodology, Investigation, Data curation, Conceptualization. **Malcolm Abbott:** Writing – review & editing, Validation, Supervision, Resources, Project administration, Methodology, Investigation, Funding acquisition, Data curation, Conceptualization. **Bram Hoex:** Writing – review & editing, Supervision, Funding acquisition, Conceptualization.

Declaration of competing interest

The authors declare the following financial interests/personal relationships which may be considered as potential competing interests:

Fiacre Rougieux reports financial support was provided by Australian Renewable Energy Agency. If there are other authors, they declare that they have no known competing financial interests or personal relationships that could have appeared to influence the work reported in this paper.

Data availability

Data will be made available on request.

Acknowledgements

This work received support from the Australian Government through the Australian Renewable Energy Agency (ARENA 1–060 Extension project). However, the Australian Government does not accept responsibility for the views, information, or advice expressed in this research.

Appendix

A.1 Impact of the width and the energy of the peak of the Gaussian distribution

The impact of charge and D_{it} is intuitive. To get a better intuition into the impact of the of the width of the Gaussian distribution and the depth of the defect energy level, we simulate their impact on injection-dependent lifetime in Figure A1. A wider distribution (Figure A1a) and deeper defects (Figure A1b) understandably lead to lower lifetimes.

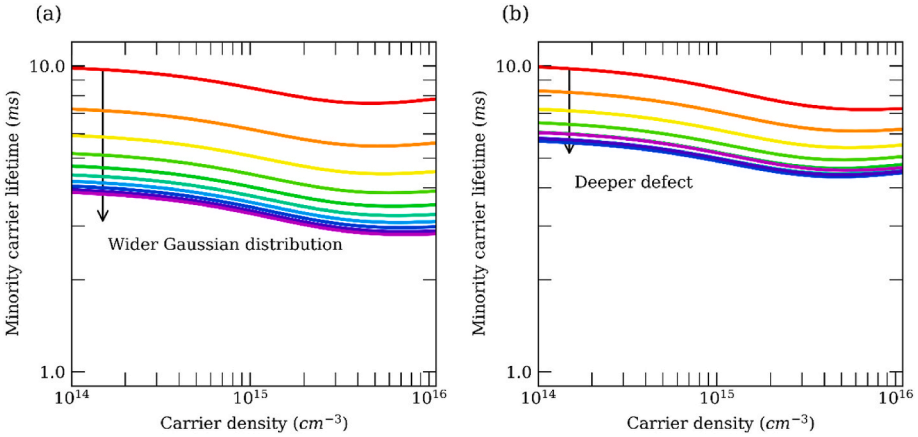

Fig. A1. Modelled impact of a) the width of the Gaussian defect distribution and b) the depth of the peak of the Gaussian defect distribution on the injection dependent minority carrier lifetime.

A.2 Impact of the capture cross section and correlation energy

To get a better intuition into the impact of the defect capture cross section and the defect correlation energy (energy between the two levels of the multivalent defect), we simulate their impact in Figure A2. Larger charged capture cross sections (Figure A2a) lead to lower lifetime, especially at low injection. Larger correlation energies (Figure A2b) lead to higher lifetimes, with the effect being more pronounced at low injection.

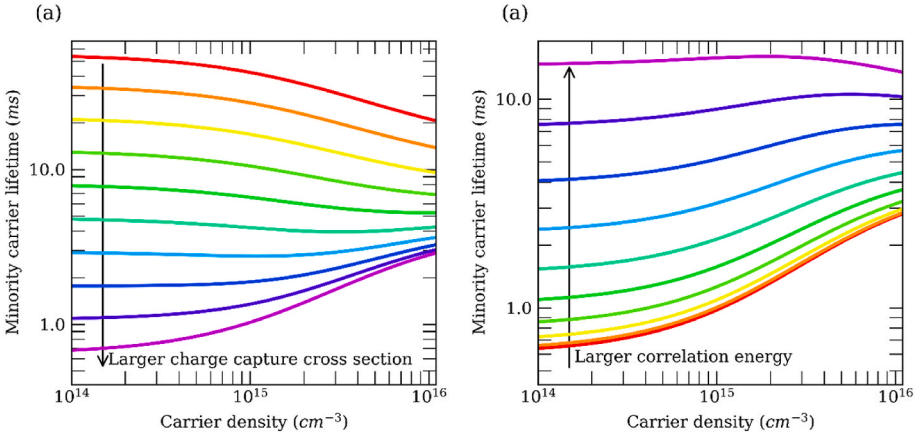

Fig. A2. Modelled impact of a) the charge capture cross section and b) the correlation energy on the injection dependent minority carrier lifetime.

A.3 Example solution space

Though the fitting is performed using the Nelder-Mead algorithm, it is useful to visualise the solution space to investigate whether it is narrow around the optimal value or if a wide range of values allows for the observed injection-dependent effective lifetime. Figure A3 shows the solution space after brute force fitting the lifetime.

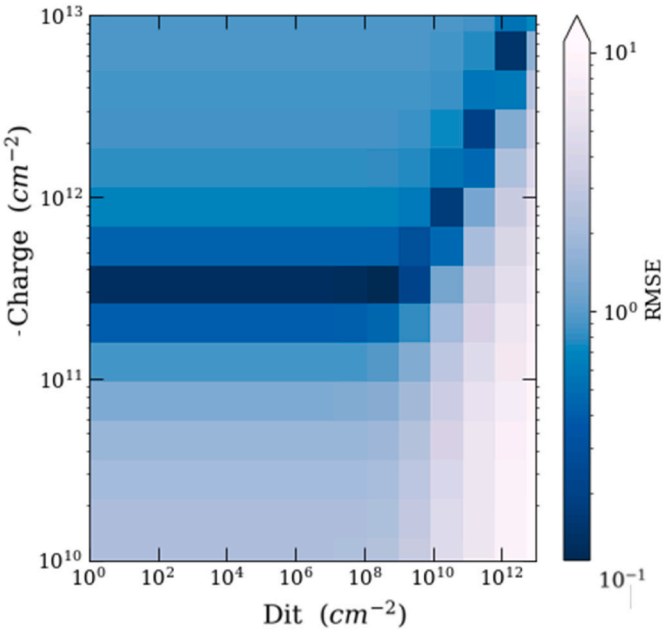

Fig. A3. Solution space after performing a brute force fitting of the lifetime.

The solution space is relatively narrow around the optimum value. When the charge or interface defect density becomes low, injection-dependent spectroscopy becomes insensitive to charge or interface density and thus the values from the optimisation.

A.4 Stability of i/p-Si

Figure A4 shows the evolution of the lifetime of the i/p-Si samples after treatment. The lifetime remains almost constant after processing.

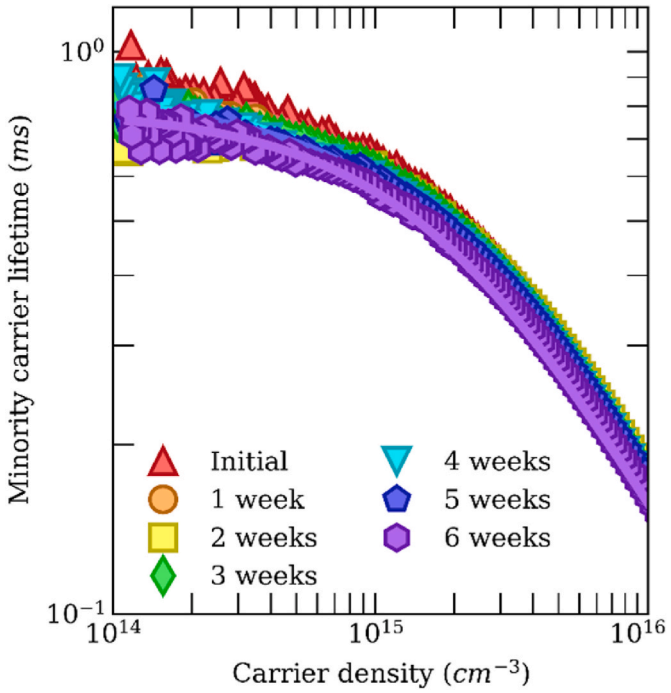

Fig. A4. i/p-Si: Evolution of the lifetime and for a sample after laser processing after different length of storage in the dark. The line is the modelled lifetime used to extract changes in charge and interface defect density.

References

[1] H. Lin, et al., Silicon heterojunction solar cells with up to 26.81% efficiency achieved by electrically optimized nanocrystalline-silicon hole contact layers, Nat. Energy 8 (8) (Aug. 2023) 789–799, https://doi.org/10.1038/s41560-023-01255-2, 8.

[2] E. Kobayashi, et al., Increasing the efficiency of silicon heterojunction solar cells and modules by light soaking, Sol. Energy Mater. Sol. Cell. 173 (Dec. 2017) 43–49, https://doi.org/10.1016/j.solmat.2017.06.023.

[3] M. Wright, et al., On the kinetics of high intensity illuminated annealing of n-type SHJ solar cells: 0.4%abs efficiency gain in one second, Sol. Energy Mater. Sol. Cell. 248 (Dec. 2022) 112039, https://doi.org/10.1016/j.solmat.2022.112039.
[4] J. Cattin, et al., Influence of light soaking on silicon heterojunction solar cells with various architectures, IEEE J. Photovoltaics 11 (3) (May 2021) 575–583, https://doi.org/10.1109/JPHOTOV.2021.3065537.
[5] S. Bao, et al., The rapidly reversible processes of activation and deactivation in amorphous silicon heterojunction solar cell under extensive light soaking, J. Mater. Sci. Mater. Electron. 32 (4) (Feb. 2021) 4045–4052, https://doi.org/10.1007/s10854-020-05146-0.
[6] P. Mahtani, R. Varache, B. Jovet, C. Longeaud, J.-P. Kleider, N.P. Kherani, Light induced changes in the amorphous—crystalline silicon heterointerface, J. Appl. Phys. 114 (12) (Sep. 2013) 124503, https://doi.org/10.1063/1.4821235.
[7] K. Wilken, M. Güneş, S. Wang, F. Finger, V. Smirnov, Understanding the origin of thermal annealing effects in low-temperature amorphous silicon films and solar cells, Phys. Status Solidi 219 (9) (2022) 2100451, https://doi.org/10.1002/pssa.202100451.
[8] X. Li, et al., Intensive light soaking improves electricity generation of silicon heterojunction solar cells by the anomalous Staebler–Wronski effect, APEX 15 (9) (Aug. 2022) 091001, https://doi.org/10.35848/1882-0786/ac8784.
[9] W. Liu, et al., Light-induced activation of boron doping in hydrogenated amorphous silicon for over 25% efficiency silicon solar cells, Nat. Energy 7 (5) (May 2022) 5, https://doi.org/10.1038/s41560-022-01018-5.
[10] L. Yang, X. Li, W. Zhang, Q. Yang, Q. Wang, On the kinetics of light-induced enhancement effect in silicon heterojunction solar cells, Phys. Status Solidi Rapid Res. Lett. 17 (3) (2023) 2200356, https://doi.org/10.1002/pssr.202200356.
[11] M. Garín, U. Rau, W. Brendle, I. Martín, R. Alcubilla, Characterization of a-Si:H/c-Si interfaces by effective-lifetime measurements, J. Appl. Phys. 98 (9) (Nov. 2005) 093711, https://doi.org/10.1063/1.2128047.
[12] W. Shockley, W.T. Read, Statistics of the recombinations of holes and electrons, Phys. Rev. 87 (5) (Sep. 1952) 835–842, https://doi.org/10.1103/PhysRev.87.835.
[13] R.N. Hall, Electron-hole recombination in germanium, Phys. Rev. 87 (2) (Jul. 1952), https://doi.org/10.1103/PhysRev.87.387, 387–387.
[14] S. Olibet, E. Vallat-Sauvain, C. Ballif, Model for a-Si:H/c-Si interface recombination based on the amphoteric nature of silicon dangling bonds, Phys. Rev. B 76 (3) (Jul. 2007) 035326, https://doi.org/10.1103/PhysRevB.76.035326.
[15] J. Hubin, A.V. Shah, E. Sauvain, Effects of dangling bonds on the recombination function in amorphous semiconductors, Phil. Mag. Lett. 66 (3) (Sep. 1992) 115–125, https://doi.org/10.1080/09500839208229273.
[16] C.-T. Sah, W. Shockley, Electron-hole recombination statistics in semiconductors through flaws with many charge conditions, Phys. Rev. 109 (4) (Feb. 1958) 1103–1115, https://doi.org/10.1103/PhysRev.109.1103.
[17] C. Leendertz, R. Stangl, T.F. Schulze, M. Schmidt, L. Korte, A recombination model for a-Si:H/c-Si heterostructures, Phys. Status Solidi C 7 (3–4) (2010) 1005–1010, https://doi.org/10.1002/pssc.200982698.
[18] C. Leendertz, N. Mingirulli, T.F. Schulze, J.P. Kleider, B. Rech, L. Korte, Discerning passivation mechanisms at a-Si:H/c-Si interfaces by means of photoconductance measurements, Appl. Phys. Lett. 98 (20) (May 2011) 202108, https://doi.org/10.1063/1.3590254.
[19] F. Werner, A. Cosceev, J. Schmidt, Interface recombination parameters of atomic-layer-deposited Al_2O_3 on crystalline silicon, J. Appl. Phys. 111 (7) (Apr. 2012) 073710, https://doi.org/10.1063/1.3700241.
[20] Z. Xin, et al., An improved methodology for extracting the interface defect density of passivated silicon solar cells, IEEE J. Photovoltaics 6 (5) (Sep. 2016) 1080–1089, https://doi.org/10.1109/JPHOTOV.2016.2576685.
[21] A.G. Aberle, S. Glunz, W. Warta, Impact of illumination level and oxide parameters on Shockley–Read–Hall recombination at the Si-SiO_2 interface, J. Appl. Phys. 71 (9) (May 1992) 4422–4431, https://doi.org/10.1063/1.350782.
[22] K.R. McIntosh, L.E. Black, On effective surface recombination parameters, J. Appl. Phys. 116 (1) (Jul. 2014) 014503, https://doi.org/10.1063/1.4886595.
[23] M.J. Powell, S.C. Deane, Defect-pool model and the hydrogen density of states in hydrogenated amorphous silicon, Phys. Rev. B 53 (15) (Apr. 1996) 10121–10132, https://doi.org/10.1103/PhysRevB.53.10121.
[24] M. Schmidt, A. Schoepke, O. Milch, T. Lussky, W. Fuhs, Photoelectron spectroscopic investigations of very thin a-Si:H layers, MRS Online Proc. Libr. 762 (Jan. 2003), https://doi.org/10.1557/PROC-762-A19.11 p. A19.11.
[25] K. Tanaka, E. Maruyama, T. Shimada, H. Okamoto, Amorphous Silicon, Wiley-Blackwell, 1999.
[26] H. Plagwitz, Surface Passivation of Crystalline Silicon Solar Cells by Amorphous Silicon Films, 2007.
[27] J.A. Nelder, R. Mead, A simplex method for function minimization, Comput. J. 7 (4) (Jan. 1965) 308–313, https://doi.org/10.1093/comjnl/7.4.308.
[28] B. Macco, et al., Correlating the silicon surface passivation to the nanostructure of low-temperature a-Si:H after rapid thermal annealing, J. Appl. Phys. 122 (3) (Jul. 2017) 035302, https://doi.org/10.1063/1.4994795.
[29] S.J. Pearton, J.W. Corbett, T.S. Shi, Hydrogen in crystalline semiconductors, Appl. Phys. A 43 (3) (Jul. 1987) 153–195, https://doi.org/10.1007/BF00615975.
[30] K. Ghosh, C.J. Tracy, S. Herasimenka, C. Honsberg, S. Bowden, Explanation of the device operation principle of amorphous silicon/crystalline silicon heterojunction solar cell and role of the inversion of crystalline silicon surface, in: 2010 35th IEEE Photovoltaic Specialists Conference, IEEE, Honolulu, HI, USA, Jun. 2010, pp. 1383–1386, https://doi.org/10.1109/PVSC.2010.5614387.
[31] C. Sun, F.E. Rougieux, D. Macdonald, A unified approach to modelling the charge state of monatomic hydrogen and other defects in crystalline silicon, J. Appl. Phys. 117 (4) (Jan. 2015) 045702, https://doi.org/10.1063/1.4906465.
[32] I.A. Kurova, N.N. Ormont, The effect of illumination on dark conductivity and photoconductivity of hydrogenated amorphous silicon layered films, Moscow Univ. Phys. 64 (5) (Oct. 2009) 527–531, https://doi.org/10.3103/S0027134909050129.
[33] S. Bowden, U. Das, S. Herasimenka, R. Birkmire, Stability of amorphous/crystalline silicon heterojunctions, in: 2008 33rd IEEE Photovoltaic Specialists Conference, May 2008, pp. 1–4, https://doi.org/10.1109/PVSC.2008.4922850.